COINCIDENT CLOUD OBSERVATIONS BY ALTIMETRY AND RADIOMETRY

Graham D. Quartly[1] and Caroline A. Poulsen[2]

[1] *Southampton Oceanography Centre, Empress Dock, Southampton, Hants, SO14 3ZH, UK. email: gdq@soc.soton.ac.uk*
[2] *Rutherford Appleton Laboratory, Chilton, Didcot, Oxon, OX11 0QX, UK. email: c.a.poulsen@rl.ac.uk*

ABSTRACT

There are many different sensors that can be used for studies of clouds or rain. However, it is only with Envisat that a dual-frequency altimeter has been co-manifested with a high-precision infra-red radiometer. This paper is the first to demonstrate the complementary cloud information obtainable from these two sensors. The examples considered here are of major storms brewing in the ITCZ just to the west of Africa. The cloud tops exceed 13 km, but much of this is inactive cirrus shield; the intense rain occurs where the optical depth exceeds 25 units.

1. INTRODUCTION

Rain is a key part of the freshwater flux between atmosphere and ocean, which has important effects upon the salinity of surface waters of the ocean. A wide variety of spaceborne sensors show sensitivity to some aspect of rain-bearing clouds, whether it be cloud tops, the frozen hydrometeors within the cloud, or the liquid precipitation itself [1]. However, often these contrasting sensors are borne on different platforms. As rain events can evolve quickly, synergistic studies are problematical due to the requirement for close match-ups in time between the different satellite passes. Envisat opens up new opportunities, with its array of sensors able to measure cloud parameters and rain at a fine spatial resolution. We consider three sensors in particular (introduced below), and show an example multi-sensor case study in section 2, with the different measurements brought together in section 3.

1.1 Radar altimeter, RA-2

The data returned by altimeters provide estimates of several oceanographic variables; the addition of a second operating frequency allows estimation of the attenuation of the signals by rain. This was first noted with TOPEX's K_u- and C-band [2], and then used to derive a rainfall climatology [3]. A similar approach is applied to the K_u-and S-band altimeter on Envisat.

The normalized backscatter, σ^0, is primarily an indicator of the roughness of the ocean surface, which is mainly due to wind. In the absence of rain there is a close correlation between the σ^0 values at the two frequencies (Fig. 1). Using this empirical mean relationship, all S-band values of σ^0 can be converted to their K_u-band equivalent. Where the observed K_u-band values lie significantly below this, there is likely to be attenuation, $\Delta\sigma^0$, due to rain (Fig. 2). Rain rate, R, (in mm h^{-1}) can be inferred using:

$$\Delta\sigma^0 \; = \; 2 \, a \, R^b \, h \qquad (1)$$

where h is the height of the column of raindrops (that the radar pulse passes through twice), and a and b are constants giving the specific attenuation. Here we use a=0.02038 dB/km, b=1.203, as suggested by Goldhirsh and Walsh [4], although the appropriate values will vary with air temperature and drop size distribution [5]. Height, h, is related to the height of the 0˚C isotherm, which can be determined from climatologies or meteorological models; in the tropics, this value is ~4.5 km year round.
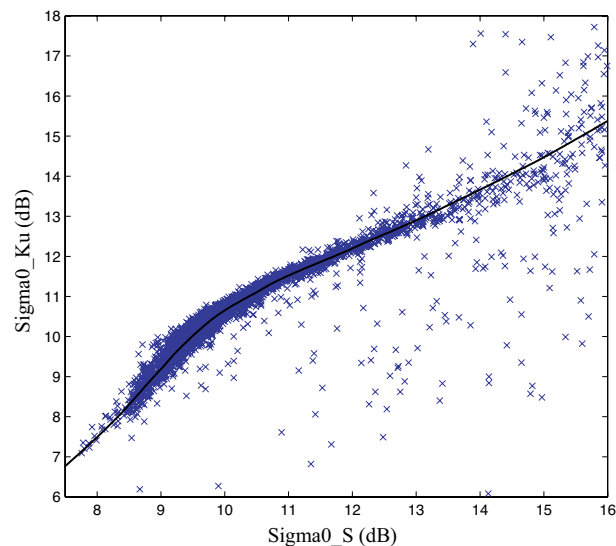

Fig. 1. Scatterplot of σ^0_{Ku} and σ^0_S, with line showing mean relationship.

1.2 Microwave radiometer, MWR

The microwave radiometer on Envisat is based closely upon the heritage of its predecessors on ERS-1 and
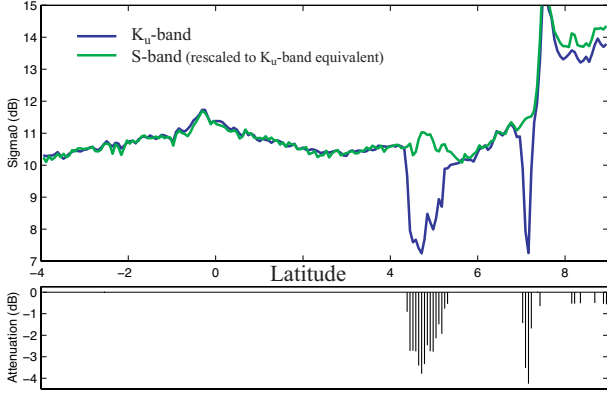
Fig. 2. a) K_u-band and S-band σ^0 values along an example profile, showing generally good agreement, with a sharp change in wind field at 7°N (high σ^0, low winds on the northern side). b) Attenuation (where significant).

ERS-2. It is not a scanning instrument, but is pointed simply along the altimeter track. The 23.8 GHz is angled slightly ahead of nadir and the 36.5 GHz aft, with both footprints having a diameter of ~20 km (Fig. 3). The primary purpose of this instrument is to provide estimates of water vapour (WV) and liquid water content (LWC), which yield important height corrections for the altimeter

A simple pair of equations has been developed [6] to determine the two derived quantities from the observed brightness temperatures, $T_{23.8}$ and $T_{36.5}$:

$$WV = a_1 \log(280-T_{23.8}) + a_2 \log(280-T_{36.5}) + a_3 + a_4 U_{10} \qquad (2)$$

$$LWC = b_1 \log(280-T_{23.8}) + b_2 \log(280-T_{36.5}) + b_3 + b_4 U_{10} \qquad (3)$$

where the wind speed, U_{10}, makes a contribution due to its effect on sea surface roughness and thus emissivity.
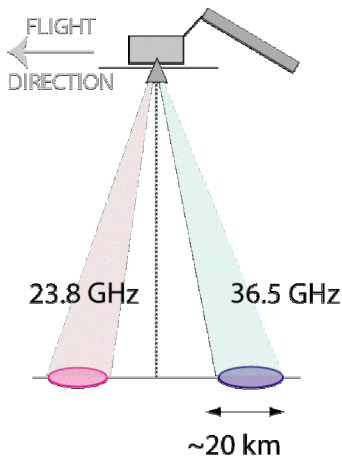

Fig. 3. Schematic illustrating viewing geometry of MWR on Envisat.

1.3 Infra-red radiometer, AATSR

The Advanced Along-Track Scanning Radiometer (AATSR) is a high-resolution radiometer giving well-calibrated data at 7 channels in the infra-red and visible bands. Although principally designed for climate studies of sea surface temperature, its data have a number of other applications.

Watts et al. [7] developed a model that estimates the cloud properties, cloud top height, optical depth and effective radius from AATSR measurements. The top of atmosphere (TOA) radiances are calculated using RTTOV for the thermal channels and MODTRAN for the shortwave channels. Cloud radiative properties are calculated for many different cloud scenarios using DISORT [8] and stored in look-up tables. Mie scattering is assumed for water droplets and ice crystals' scattering properties are calculated using a combination of geometric optics and the T-matrix method. The results are then combined into two three-layer models (Fig. 4).
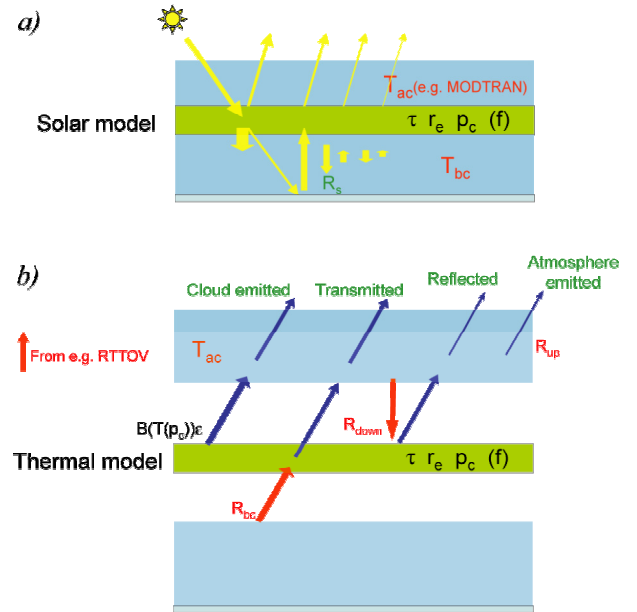

Fig. 4. Schematics of fluxes within layered cloud model. a) Solar model, b) Thermal model. (Details of the terms in figure can be found in Watts et al. [7].)

For each AATSR measurement the optimal set of cloud parameters is found by minimizing a cost function:

$$J = [y_m - y(x_n)] S_y^{-1} [y_m - y(x_n)]^T + [x_n - x_b] S_x^{-1} [x_n - x_b]^T \qquad (4)$$

where y_m are the radiances, S_y the measurement error covariance and $y(x_n)$ the cloud parameters modeled into radiance space, X_b is the *a priori* and S_x the *a priori* covariance. The technique is able to incorporate any *a priori* information such as ECMWF temperature

and humidity profiles and surface albedo. This
approach also provides estimates of the error in each
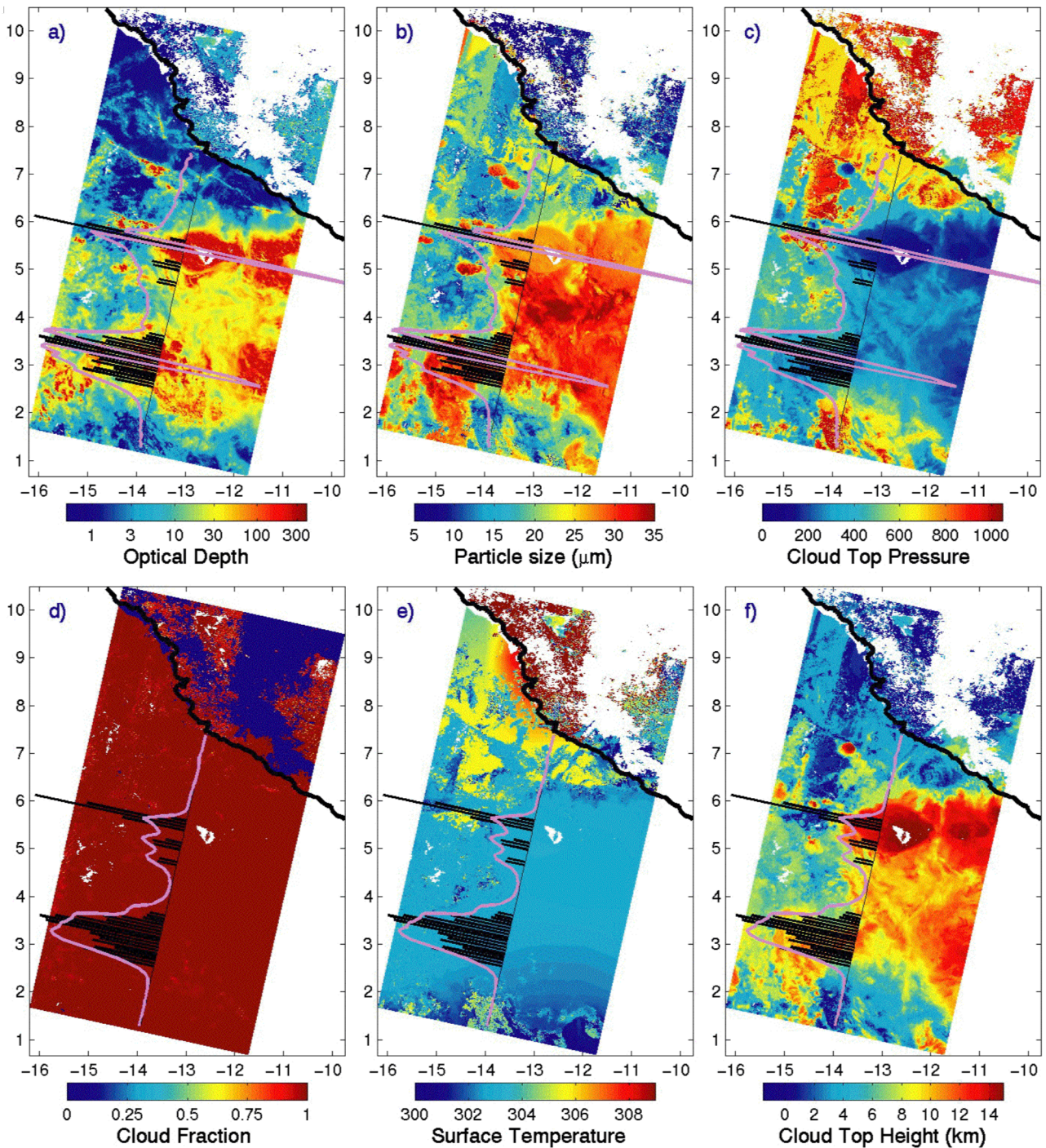parameter.

Fig. 5. Cloud parameters for an AATSR swath of 11th May 2003 heading southward from Sierra Leone (W. Africa), with rain rate indicated by black bars perpendicular to the track. Surface temperature is only directly retrievable from AATSR data where cloud is thin; elsewhere, this field shows the *a priori* from ECMWF. Top row also includes a pink line indicating WV-50 kg m^{-2}; in the bottom row it represents LWC. (See Fig. 6 for the quantitative values for rain rate, WV and LWC.)

2. CASE STUDY OFF WEST AFRICA

Six examples of extreme rain events were noted from altimeter data, and the corresponding AATSR level 1b data acquired and processed. The six inferred cloud parameters are shown for a particular case study (Fig. 5), with the coincident RA-2 and MWR data overlaid along the nadir track. The altimeter footprint is roughly a disc 8 km in diameter; cloud parameters derived from the AATSR inversion are averaged to this resolution for comparison along the transect of the storm; a subset is shown in Fig. 6.
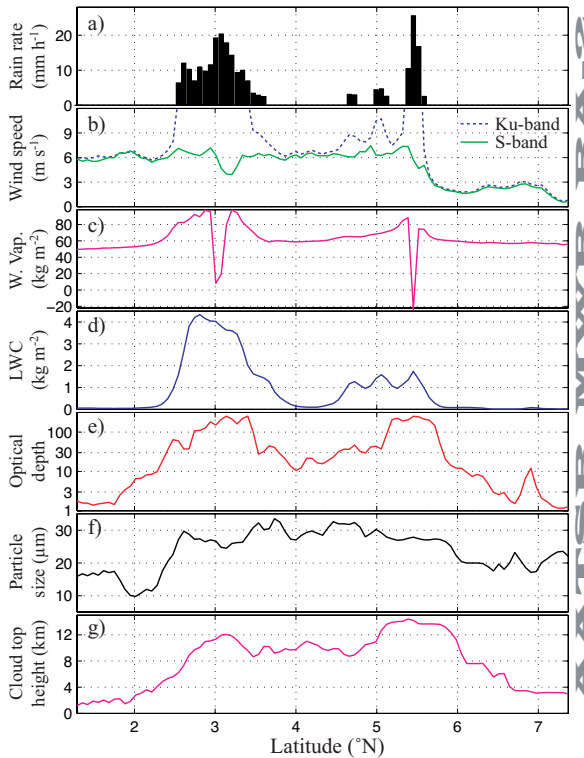

Fig. 6. Profile of key cloud/rain parameters plus surface wind speed along nadir track shown in Fig. 5. (AATSR data have been smoothed to resolution of RA-2.)

Nearly all of the individual 1 km pixels in the swath are designated 100% cloudy (Fig. 5d), and much of the region between 2.5°N and 6°N has cloud tops above 10 km, with an effective radius (Fig. 5b) of around 30 μm. However, the RA-2 and MWR show much more confined regions of activity, with the rain and high LWC principally in the bands 2.5°-3.5°N and 4.5°-5.5°N, which are the regions where the optical depth is greatest.

Note, the event illustrated challenged the inversion algorithms of all the sensors. The standard altimeter wind algorithm is based on σ^0_{Ku}; however the pronounced attenuation (more than 7 dB at 3°N and 5.5°N) leads to very high wind speed estimates. Here

we also show the wind speed based on the σ^0_S values as they are hardly affected. The brightness temperature measurements of the MWR record realistically high values over the two events (not shown); however, the derived WV values in the centre of these events are not believable. This is probably because the standard ESA processing uses anomalously large wind speed values in (2), with these U_{10} values being determined from σ^0_{Ku}. The optimal inversion of the AATSR data generally works well, but the derived optical depth values are capped at 256 as that was the limit of the simulated conditions used to populate the look-up tables. Also, there are regions just off the nadir track at 5.5°N for which no inversion is possible, because the cloud top was so cold that the measurements at 11 μm and 12 μm were set to 'invalid'.

3. COMBINING DATA FROM DIFFERENT SENSORS

Of the various AATSR-derived cloud parameters, optical depth (OD) is the one that shows the closest correspondence to the rain cells detected by RA-2. Bringing together the six case studies identified in this region (all with peak rain rates exceeding 12 mm h^{-1}), we produce a scatterplot of OD and attenuation (Fig. 7). Because of uncertainties in the altimeter estimates
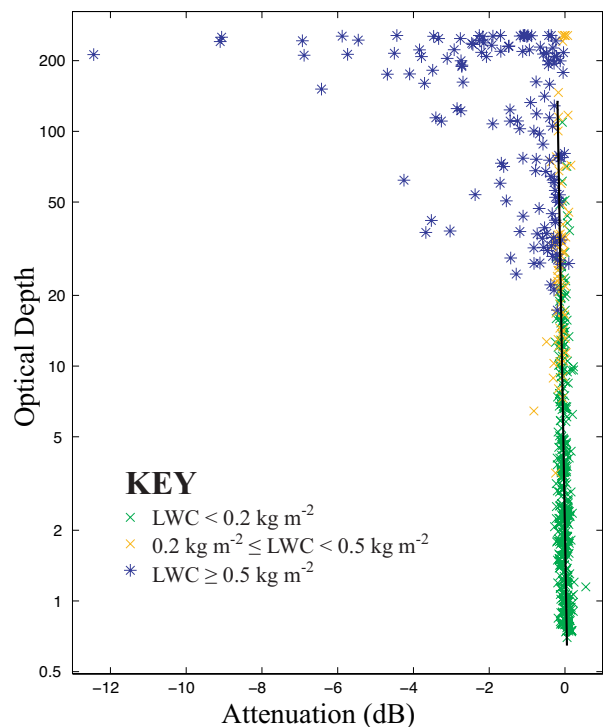

Fig. 7. Scatterplot of Optical Depth (from AATSR) against attenuation (from RA-2) sorted by LWC (from MWR). Data are for 6 intense storms off W. Africa during May 2003.

of σ^0_{Ku} and σ^0_S, the derived attenuation, $\Delta\sigma^0$ needs to be less than -0.5 dB for a clear detection of rain ($R > 2.3$ mm hr^{-1}, for h=4.5 km). In the cases shown this condition is not exceeded unless

$$OD > 25 \;\; \text{AND} \;\; LWC \geq 0.5 \text{ kg m}^{-2} \qquad (5)$$

The black line indicating the mean relationship of $\Delta\sigma^0$ and $\log_{10}(OD)$ for LWC<0.5 kg m^{-2} is not quite vertical, but corresponds to:

$$\log_{10}(OD) = -9.28 \, \Delta\sigma^0 + 0.27 \qquad (6)$$
or
$$k_{opt} / k_{Ku} = 92.8 \qquad (7)$$

where k_{opt} and k_{Ku} are the specific attenuations for non-raining clouds at optical frequencies (centred on 0.55 µm) and K$_u$-band.
The ratio of specific attenuations (7) and the OD and LWC thresholds for rain (5) may be particular to the large storms developing in this tropical location. We plan to develop this analysis for other regions.

4. CONCLUSIONS AND FURTHER WORK

We have examined six intense storms off the west coast of Africa; the nature of the selected events was so extreme that some pixels in the AATSR swath were outside the range of scenarios used to populate the look-up tables accessed in the inversion. The effect of intense rain on σ^0_{Ku} (and thus the derived K$_u$-band wind speed) has been well documented before; here we note the effect on standard MWR retrievals of WV. A more robust approach would be to use a wind speed calculated from σ^0_S, enabling realistic WV profiles across major storms.
All six cases showed that rain coincided most closely with OD and LWC. Significant rain is associated with OD > 25 and LWC $\geq$ 0.5 kg m^{-2}, but rain rates cannot, in general, be accurately determined from those two measurements. It may be that AATSR swath information can be used to extrapolate the altimeter rain rates from the nadir track; however, it seems unlikely that the AATSR data can give reliable rain rates in the absence of local specific measurements by the dual-frequency altimeter.

This study has shown that synergistic use of sensors onboard Envisat has the potential to provide extra information on the rain rates of convective clouds. For example the altimeter can discriminate the active convective regions from the higher lying shield of remnant cirrus. We now plan to examine storms and frontal rain in other locations, specifically mid and high latitudes, in order to understand better how to use the suite of cloud/rain sensors on Envisat.

6. REFERENCES

1. Quartly, G.D., T.H. Guymer and M.A. Srokosz, Back to basics: Measuring rainfall at sea. Part 2 - Space-borne sensors, *Weather*, Vol. 57, 363-366, 2002.
2. Quartly G.D., T.H. Guymer, and M.A. Srokosz, The effects of rain on Topex radar altimeter data. *J. Atmos. Oceanic Tech.*, Vol. 13, 1209-1229, 1996.
3. Quartly G.D., M.A. Srokosz, and T.H. Guymer, Global precipitation statistics from dual-frequency TOPEX altimetry. *J. Geophys. Res.*, Vol. 104, 31489-31516, 1999.
4. Goldhirsh, and E.J. Walsh, Rain measurements from space using a modified Seasat-type radar altimeter, *IEEE Trans. Antennas. Propag.* Vol. 30, 726-733, 1982.
5. Slack, J.K., A.R. Holt, and V. Brown, Workpackage WP 400: Implementation of direct algorithms, in *Rain radar retrieval algorithms*, edited by J. Testud, ESA contract 10146/92/NL/GS, 1994.
6. Eymard, L., A. Le Cornec, and L. Tabary, The ERS-1 microwave radiometer. *Int. J. Remote Sensing*, Vol. 15, 845-857, 1994.
7. Watts, P.D. et al., Study on cloud properties derived from Meteosat Second Generation observations. EUMETSAT ITT no. 97/181, 1998.
8. Wiscombe et al., DISORT, discrete ordinates method code, *Applied Optics*, Vol. 27 no. 12, 1988.